AIAA SciTech Forum
8-12 January 2024, Orlando, FL
AIAA SCITECH 2024 Forum

10.2514/6.2024-0286

On the Formulation of the Resolvent Operator for Compressible Flows

Diganta Bhattacharjee* and Maziar S. Hemati†
University of Minnesota, Minneapolis, MN 55455, USA

This paper investigates the non-uniqueness of resolvent analysis in the context of compressible fluid flows. Specifically, we compare two mathematically equivalent formulations of the compressible Navier-Stokes equations (NSEs) in two sets of flow variables related via a nonlinear transformation, which we refer to as the 'Cubic+' and 'Quadratic+' formulations. The Cubic+ formulation is based on the conventional representation of compressible NSEs using the primitive variables of density, velocity components and temperature, whereas the Quadratic+ formulation utilizes a representation where density and temperature are replaced by specific volume and pressure, respectively. These formulations are implemented on a compressible plane Couette flow for a broad range of Mach numbers. Although the Quadratic+ formulation generally predicts higher amplifications than the Cubic+ formulation when the Chu energy is utilized for the compressible inner product, this trend reverses if kinetic energy is instead used to define the inner product. Furthermore, for some combinations of the streamwise and spanwise wavenumber pairs, the two formulations predict substantially different temporal behaviors. These range from differences in estimating the temporal frequencies for the largest gains to instances wherein one formulation predicts a single global peak when the other predicts multiple local peaks. In addition, the Quadratic+ results feature localized regions of wavenumber space associated with high resolvent gains that are absent in the Cubic+ results, but are qualitatively comparable to one another otherwise. The inconsistencies observed in resolvent analysis based on the two formulations considered here suggest that any insights drawn from resolvent analysis should be accompanied by computational and/or experimental studies to corroborate findings and interpretations of the underlying physics.

I. Introduction

Developing a comprehensive understanding of the flow physics of high-speed fluid flows, which are governed by the compressible Navier-Stokes equations (NSEs), is a key component for aerospace applications going forward. In this regard, conducting high-fidelity numerical experiments using computational fluid mechanics tools are now a viable option due to the advances in super-computing technology in the last few decades. Especially in the context of turbulent flows, direct numerical simulations has proven to be a powerful numerical tool, but its applicability for a broad range of parameters–primarily, Reynolds number and Mach number–remains somewhat limited despite recent progress [1, 2]. Alternative to the numerical experiments, model-based frameworks like input-output (I/O) methods have been successful in providing important insight into the flow physics and have been useful in uncovering key mechanisms of instability in the incompressible regime [3, 4] and are getting increasingly popular for analyzing high-speed compressible flows as well [1, 2, 5–8].

In the context of flow instability and transition to turbulence, the equations governing the fluid flow can be expressed as a feedback interconnection between a linear system and a nonlinear mapping (see, for example, the schematic in Fig. 1a). Now, resolvent analysis [10, 11], like all other linear I/O methods, removes the aforementioned feedback interconnection and replaces the nonlinear terms by some implicit forcing on the linear dynamics (compare the Figs. 1c and 1a), which greatly simplifies the subsequent analysis. We recently extended an I/O method–called the structured I/O analysis [12]–to the compressible flows in Ref. [9]. Instead of removing the feedback nonlinearity altogether, the structured I/O modeling introduces pseudo-linear approximations for the nonlinear (quadratic) terms [9, 12] (compare the schematics shown in Figs. 1b and 1a). The structured I/O analysis is based upon the concept of structured singular value [13] from robust control theory. In Ref. [9], we implemented the structured I/O framework for compressible flows on a compressible plane Couette flow and compared the results with those obtained from an equivalent resolvent

*Postdoctoral Research Associate, Department of Aerospace Engineering and Mechanics, AIAA Member.
†Associate Professor, Department of Aerospace Engineering and Mechanics, AIAA Associate Fellow.

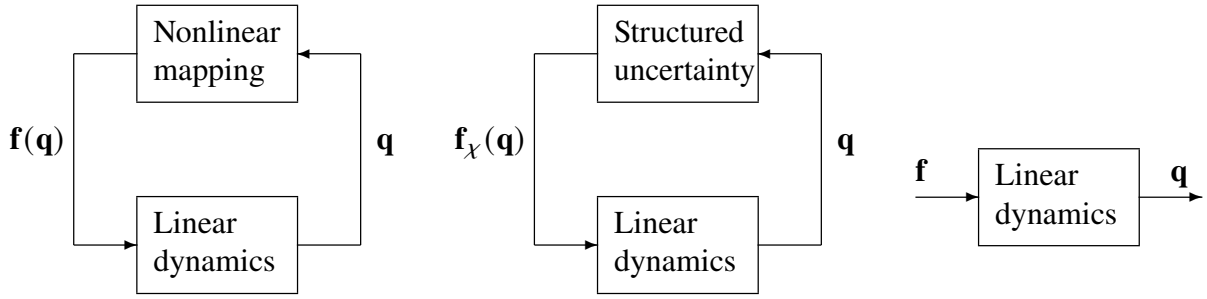

(a) Actual nonlinear system **(b) Structured I/O system** **(c) Linearized system**

Fig. 1 Stability of transitional fluid flows and the governing equations of perturbations (q) about a steady base flow. These equations are shown in three different forms: (a) the original system with the linear dynamics in feedback with the nonlinearity $\mathbf{f}(\mathbf{q})$; (b) the structured I/O modeling with $\mathbf{f}_\chi(\mathbf{q})$ representing the approximated nonlinearity (see Ref. [9] for details); (c) the linearized system obtained by removing the aforementioned feedback connection.

analysis. The comparison revealed several contradictory aspects about the instability mechanisms associated with the flow [9]. Although the structured I/O modeling is an obvious source of the discrepancies reported in Ref. [9], another possibility is the choice of variables used to describe the flow, as pointed out in Ref. [14]. The theoretical developments and case studies in Ref. [14] established that resolvent analysis–or indeed any I/O analysis based on the linearization of nonlinear NSEs about a base or mean flow–might lead to substantially different results for different choices of the flow variables describing the same flow. This ambiguity, coupled with the discrepancies noticed in our prior work (Ref. [9]), serves as a motivation for the study reported in this paper.

We start by linearizing the compressible NSEs described in terms of two sets of primitive variables. When working with the primitive variables of density, velocity components and temperature, the resulting linearized equations are termed 'Cubic+'. The other representation–which replaces density and temperature with specific volume and pressure, respectively–leads to the 'Quadratic+' formulation of linearized equations. The corresponding resolvent operators are then implemented on a compressible Couette flow for a wide range of Mach numbers. Despite qualitative similarities between the two sets of results, we have identified several combinations of the streamwise and spanwise wavenumber pairs where the results differ substantially, predicting significantly different temporal behaviors of the linearized flow dynamics.

The remainder of the paper proceeds as follows: the linearized formulations of compressible NSEs are discussed in Section II. Details of the resolvent analysis and simulation results for a compressible plane Couette flow are given in Section III. Section IV provides the concluding remarks and future directions of research.

II. Linearization of Compressible Navier-Stokes Equations

In this section, we describe two sets of linearized equations of flow perturbations about a steady base flow based on two mathematically equivalent representations of the compressible NSEs. These representations include the conventional one typically used for I/O methods in the literature [1, 5, 6] and the specific one we outlined for structured I/O analysis in [9]. Let us consider a compressible fluid in the domain $\Omega \subset \mathbb{R}^3$, and use $\mathbf{x} \in \Omega$ and $t \in \mathbb{R}_{\geq 0}$ to denote the spatial coordinates and time, respectively. The state of the fluid at any instant in time can be characterized solely based on one of the following sets of primitive variables: (i) density $\rho(\mathbf{x}, t)$, velocity $\mathbf{u}(\mathbf{x}, t) = (u(\mathbf{x}, t), v(\mathbf{x}, t), w(\mathbf{x}, t))$, and temperature $T(\mathbf{x}, t)$; (ii) specific volume $\xi(\mathbf{x}, t) = 1/\rho(\mathbf{x}, t)$, velocity $\mathbf{u}(\mathbf{x}, t) = (u(\mathbf{x}, t), v(\mathbf{x}, t), w(\mathbf{x}, t))$, and pressure $p(\mathbf{x}, t)$. Then, the fundamental principles of mass, momentum and energy conservation are applied to derive the equations governing the dynamics of the flow in Ω.

A. Cubic+ Formulation

Let us first consider the non-dimensionalized compressible NSE in the variables $\mathbf{q}_c = (\rho, \mathbf{u}, T) = (\rho, u, v, w, T)$, i.e., the conventional description widely used in the literature [1, 5, 6]. These are given by

$$\begin{aligned}
\partial_t \rho + \nabla \cdot (\rho \mathbf{u}) &= 0 \\
\rho \left(\partial_t \mathbf{u} + \mathbf{u} \cdot \nabla \mathbf{u}\right) &= -\frac{1}{\gamma M_r^2} \nabla p + \frac{1}{Re} \nabla \cdot \Pi(\mathbf{u}, \eta, \lambda) \\
\rho \left(\partial_t T + \mathbf{u} \cdot \nabla T\right) &= (1-\gamma) p (\nabla \cdot \mathbf{u}) + \frac{\gamma}{RePr} \nabla \cdot (\eta \nabla T) + \frac{\gamma(\gamma-1)M_r^2}{Re} \Phi(\mathbf{u}, \eta, \lambda)
\end{aligned} \tag{1}$$

with the non-dimensional equation of state for a perfect polytropic gas $p = \rho T$. Here, Re, Pr and M_r denote the Reynolds number, Prandtl number, and Mach number, respectively. Also, $\Pi(\mathbf{u}, \eta, \lambda)$ is the viscous stress tensor and can be expressed as

$$\Pi(\mathbf{u}, \eta, \lambda) = \eta(\nabla \mathbf{u} + (\nabla \mathbf{u})^{\mathrm{T}}) + \lambda(\nabla \cdot \mathbf{u})\mathbf{I}$$

where η and λ are the first and second coefficient of viscosity, respectively. The term $\Phi(\mathbf{u}, \eta, \lambda)$ in (1) is the viscous dissipation term given by

$$\begin{aligned}
\Phi(\mathbf{u}, \eta, \lambda) &= \eta \left(2\left((\partial_x u)^2 + (\partial_y v)^2 + (\partial_z w)^2\right) + (\partial_y u + \partial_x v)^2 + (\partial_z v + \partial_y w)^2 + (\partial_z u + \partial_x w)^2\right) + \lambda(\nabla \cdot \mathbf{u})^2 \\
&= \frac{\eta}{2}\left[\nabla \mathbf{u} + (\nabla \mathbf{u})^{\mathrm{T}}\right]^2 + \lambda(\nabla \cdot \mathbf{u})^2.
\end{aligned}$$

Also, each row of the vector $\nabla \cdot \Pi(\mathbf{u}, \eta, \lambda)$ can be expressed as [5, 15]

$$\begin{aligned}
(\nabla \cdot \Pi(\mathbf{u}, \eta, \lambda))_{x_i} &= \eta \nabla^2 u_i + \partial_{x_i}\left(\lambda(\nabla \cdot \mathbf{u})\right) + \eta \partial_{x_i}(\nabla \cdot \mathbf{u}) + (\nabla \eta) \cdot (\nabla u_i) + (\nabla \eta) \cdot \partial_{x_i} \mathbf{u} \\
&= \eta \nabla^2 u_i + (\eta + \lambda)\partial_{x_i}(\nabla \cdot \mathbf{u}) + \partial_{x_i} \lambda\,(\nabla \cdot \mathbf{u}) + (\nabla \eta) \cdot (\nabla u_i) + (\nabla \eta) \cdot \partial_{x_i} \mathbf{u}
\end{aligned}$$

where x_i represents the three coordinates of $\mathbf{x}$. Throughout the remainder of the paper, we assume $\lambda = -2/3\eta$ using Stokes' hypothesis. The temperature dependence of viscosity is modeled through the Sutherland's law, given by [15]

$$\eta(T) = \frac{T^{3/2}(1+C)}{T+C} \tag{2}$$

where the constant $C = 0.5$. Note that all the non-viscous nonlinear terms in (1) are either quadratic or cubic in the variables, with the viscosity-dependent nonlinear terms taking non-integer orders due to the Sutherland's law in (2). It is for this reason we refer to the linearized dynamics obtained from (1) as the 'Cubic+' formulation in this paper.

Next, we consider the dynamics of perturbations about a steady base flow $(\rho_0, \mathbf{u}_0, p_0, T_0, \eta_0)$ with $\mathbf{u}_0 = (U_0(y), 0, 0)$. The steady base flow equations are given by

$$\begin{aligned}
\frac{d}{dy}\left(\eta_0 \frac{dU_0}{dy}\right) &= 0 \\
\frac{dp_0}{dy} &= 0 \Rightarrow p_0 = 1 \\
Pr^{-1} \frac{d}{dy}\left(\eta_0 \frac{dT_0}{dy}\right) + (\gamma-1) M_r^2 \eta_0 \left(\frac{dU_0}{dy}\right)^2 &= 0
\end{aligned} \tag{3}$$

along with the equation of state $\rho_0 T_0 = 1$ (since we have scaled the constant pressure as $p_0 = 1$). The linearized dynamics of the perturbed flow states about this base flow are summarized in the following:

$$\begin{aligned}
\partial_t \rho &= -U_0 \partial_x \rho - v \rho_0' - \rho_0 \nabla \cdot \mathbf{u} + f_{c_\rho} \\
\partial_t u &= -U_0 \partial_x u - v U_0' - \frac{1}{\gamma M_r^2}\left(T_0^2 \partial_x \rho + \partial_x T\right) + \frac{T_0}{Re}\Big(\eta_{TT_0} T_0' U_0' T + \eta_{T_0} U_0' \partial_y T + \eta_{T_0} U_0'' T \\
&\quad + \eta_0 \nabla^2 u + (\eta_0 + \lambda_0)\partial_x(\nabla \cdot \mathbf{u}) + \eta_0'\left(\partial_x v + \partial_y u\right)\Big) + f_{c_u} \\
\partial_t v &= -U_0 \partial_x v - \frac{1}{\gamma M_r^2}\left(T_0^2 \partial_y \rho + T_0 \rho T_0' + T_0 T \rho_0' + \partial_y T\right)
\end{aligned}$$

$$+\frac{T_0}{Re}\left(\eta_{T_0}U_0'\partial_x T+\eta_0\nabla^2 v+(\eta_0+\lambda_0)\partial_y(\nabla\cdot\mathbf{u})+\lambda_0'(\nabla\cdot\mathbf{u})+2\eta_0'\partial_y v\right)+f_{c_v} \tag{4}$$

$$\partial_t w=-U_0\partial_x w-\frac{1}{\gamma M_r^2}\left(T_0^2\partial_z\rho+\partial_z T\right)+\frac{T_0}{Re}\left(\eta_0\nabla^2 w+(\eta_0+\lambda_0)\partial_z(\nabla\cdot\mathbf{u})+\eta_0'\left(\partial_z v+\partial_y w\right)\right)+f_{c_w}$$

$$\partial_t T=-U_0\partial_x T-vT_0'+T_0(1-\gamma)(\nabla\cdot\mathbf{u})+\frac{T_0\gamma}{RePr}\left(\eta_{T_0}T_0''+\eta_{TT_0}(T_0')^2+2\eta_0'\partial_y+\eta_0\nabla^2\right)T$$

$$+\frac{T_0\gamma(\gamma-1)M_r^2}{Re}\left(2\eta_0U_0'(\partial_x v+\partial_y u)+\eta_{T_0}(U_0')^2T\right)+f_{c_T}$$

where all the nonlinear terms are collected in $f_{(\cdot)}$s and η_{T_0}, η_{TT_0} are the first and second derivatives, respectively, of $\eta(T)$ with respect to T and evaluated at $T = T_0$. Also, $(\cdot)'$ and $(\cdot)''$ respectively mean $d(\cdot)/dy$ and $d^2(\cdot)/dy^2$ for the associated base flow quantities. The linearized perturbation dynamics (4) can be expressed in a more compact form as

$$\partial_t\mathbf{q}_c=\mathbf{L}_c\mathbf{q}_c+\mathbf{f}_c \tag{5}$$

where $\mathbf{f}_c=\left(f_{c_\rho},f_{c_u},f_{c_v},f_{c_w},f_{c_T}\right)$ denotes the forcing and the linear operator $\mathbf{L}_c$ is

$$\mathbf{L}_c=\begin{bmatrix}L_{c_{\rho\rho}} & L_{c_{\rho u}} & L_{c_{\rho v}} & L_{c_{\rho w}} & L_{c_{\rho T}}\\ L_{c_{u\rho}} & L_{c_{uu}} & L_{c_{uv}} & L_{c_{uw}} & L_{c_{uT}}\\ L_{c_{v\rho}} & L_{c_{vu}} & L_{c_{vv}} & L_{c_{vw}} & L_{c_{vT}}\\ L_{c_{w\rho}} & L_{c_{wu}} & L_{c_{wv}} & L_{c_{ww}} & L_{c_{wT}}\\ L_{c_{T\rho}} & L_{c_{Tu}} & L_{c_{Tv}} & L_{c_{Tw}} & L_{c_{TT}}\end{bmatrix}$$

with each sub-operator given by

$$\begin{aligned}
&L_{c_{\rho\rho}}=-U_0\partial_x, L_{c_{\rho u}}=-\rho_0\partial_x, L_{c_{\rho v}}=-\rho_0'-\rho_0\partial_y, L_{c_{\rho w}}=-\rho_0\partial_z, L_{c_{\rho T}}=0, L_{c_{u\rho}}=-\frac{1}{\gamma M_r^2}T_0^2\partial_x,\\
&L_{c_{uu}}=-U_0\partial_x+\frac{T_0}{Re}\left(\eta_0\nabla^2+(\eta_0+\lambda_0)\partial_{xx}+\eta_0'\partial_y\right), L_{c_{uv}}=-U_0'+\frac{T_0}{Re}\left((\eta_0+\lambda_0)\partial_{xy}+\eta_0'\partial_x\right),\\
&L_{c_{uw}}=\frac{T_0}{Re}\left((\eta_0+\lambda_0)\partial_{xz}\right), L_{c_{uT}}=-\frac{1}{\gamma M_r^2}\partial_x+\frac{T_0}{Re}\left(\eta_{TT_0}T_0'U_0'+\eta_{T_0}U_0'\partial_y+\eta_{T_0}U_0''\right),\\
&L_{c_{v\rho}}=-\frac{1}{\gamma M_r^2}\left(T_0^2\partial_y+T_0T_0'\right), L_{c_{vu}}=\frac{T_0}{Re}\left((\eta_0+\lambda_0)\partial_{xy}+\lambda_0'\partial_x\right),\\
&L_{c_{vv}}=-U_0\partial_x+\frac{T_0}{Re}\left(\eta_0\nabla^2+(\eta_0+\lambda_0)\partial_{yy}+\lambda_0'\partial_y+2\eta_0'\partial_y\right), L_{c_{vw}}=\frac{T_0}{Re}\left((\eta_0+\lambda_0)\partial_{yz}+\lambda_0'\partial_z\right),\\
&L_{c_{vT}}=-\frac{1}{\gamma M_r^2}\left(T_0\rho_0'+\partial_y\right)+\frac{T_0}{Re}\left(\eta_{T_0}U_0'\partial_x\right), L_{c_{w\rho}}=-\frac{1}{\gamma M_r^2}\left(T_0^2\partial_z\right), L_{c_{wu}}=\frac{T_0}{Re}(\eta_0+\lambda_0)\partial_{xz},\\
&L_{c_{wv}}=\frac{T_0}{Re}\left((\eta_0+\lambda_0)\partial_{yz}+\eta_0'\partial_z\right), L_{c_{ww}}=-U_0\partial_x+\frac{T_0}{Re}\left(\eta_0\nabla^2+(\eta_0+\lambda_0)\partial_{zz}+\eta_0'\partial_y\right),\\
&L_{c_{wT}}=-\frac{1}{\gamma M_r^2}\partial_z, L_{c_{T\rho}}=0, L_{c_{Tu}}=T_0(1-\gamma)\partial_x+\frac{T_0\gamma(\gamma-1)M_r^2}{Re}\left(2\eta_0U_0'\partial_y\right),\\
&L_{c_{Tv}}=T_0(1-\gamma)\partial_y+\frac{T_0\gamma(\gamma-1)M_r^2}{Re}\left(2\eta_0U_0'\partial_x\right)-T_0', L_{c_{Tw}}=T_0(1-\gamma)\partial_z,\\
&L_{c_{TT}}=\frac{T_0\gamma}{RePr}\left(\eta_{T_0}T_0''+\eta_{TT_0}(T_0')^2+2\eta_0'\partial_y+\eta_0\nabla^2\right)+\frac{\gamma(\gamma-1)M_r^2T_0}{Re}\eta_{T_0}(U_0')^2-U_0\partial_x.
\end{aligned} \tag{6}$$

It should be noted here that $(\eta_0+\lambda_0)=1/3\eta_0$ due to Stokes' hypothesis.

B. Quadratic+ Formulation

The compressible NSEs can alternatively be described in terms of the set of primitive variables $\mathbf{q}_q=(\xi:=1/\varrho,\mathbf{u},p)$ (see Ref. [9] for details). The resulting non-dimensional equations can be expressed as [9]

$$\partial_t\xi+\mathbf{u}\cdot\nabla\xi-\xi\nabla\cdot\mathbf{u}=0$$

$$\partial_t \mathbf{u} + \mathbf{u}\cdot\nabla\mathbf{u} = -\frac{1}{\gamma M_r^2}\xi\nabla p + \frac{1}{Re}\xi\nabla\cdot\Pi(\mathbf{u},\eta,\lambda) \tag{7}$$
$$\partial_t p + \mathbf{u}\cdot\nabla p + \gamma p\nabla\cdot\mathbf{u} = \frac{\gamma(\gamma-1)M_r^2}{Re}\Phi(\mathbf{u},\eta,\lambda) + \frac{\gamma}{RePr}\nabla\cdot(\eta\nabla(p\xi))$$

with the associated non-dimensional equation of state for a perfect polytropic gas $p\xi = T$. Similar to our earlier remarks on the governing equations for the Cubic+ formulation, all the non-viscous nonlinear terms in (7) are quadratic, while the viscous nonlinearities are of fractional order due to the viscosity modeling through the Sutherland's law in (2). Therefore, we refer to the linearized dynamics obtained from (7) as the 'Quadratic+' formulation here.

Now, for a steady base flow with $(\xi_0, U_0(y), 0, 0, p_0, T_0, \eta_0)$, the base flow equations are given by

$$\frac{d}{dy}\left(\eta_0\frac{dU_0}{dy}\right) = 0$$
$$\frac{dp_0}{dy} = 0 \Rightarrow p_0 = 1$$
$$(\gamma-1)M_r^2\eta_0\left(\frac{dU_0}{dy}\right)^2 + Pr^{-1}\frac{d}{dy}\left(\eta_0\frac{d\xi_0}{dy}\right) = 0$$

along with the equation of state $\xi_0 = T_0$ since the constant pressure is again scaled as $p_0 = 1$. Thus, the above base flow equations are the same as in (3). In Ref. [9], we only allowed the viscosity associated with the base flow to be a function of the base flow temperature (i.e., $\eta_0 = \eta_0(T_0)$) and perturbations to the base viscosity η_0 were neglected. This simplification was made so that the nonlinearity in the perturbation equations were quadratic in the perturbed flow variables. This was crucial in the pseudo-linear structured I/O modeling and the subsequent analysis in Ref. [9]. However, it should be noted that no such assumption is made here and we allow viscosity perturbations as dictated by the Sutherland's law in (2). After carrying out a similar set of calculation as we previously did for the Cubic+ formulation, we can express the linearized perturbation dynamics about the base flow as

$$\partial_t \mathbf{q}_q = \mathbf{L}_q\mathbf{q}_q + \mathbf{f}_q \tag{8}$$

where $\mathbf{f}_q$ is the forcing (see $\mathbf{f}_c$ in (5) for comparison) and the linear operator $\mathbf{L}_q$ takes the following form:

$$\mathbf{L}_q = \begin{bmatrix} L_{q_{\xi\xi}} & L_{q_{\xi u}} & L_{q_{\xi v}} & L_{q_{\xi w}} & L_{q_{\xi p}} \\ L_{q_{u\xi}} & L_{q_{uu}} & L_{q_{uv}} & L_{q_{uw}} & L_{q_{up}} \\ L_{q_{v\xi}} & L_{q_{vu}} & L_{q_{vv}} & L_{q_{vw}} & L_{q_{vp}} \\ L_{q_{w\xi}} & L_{q_{wu}} & L_{q_{wv}} & L_{2_{ww}} & L_{2_{wp}} \\ L_{q_{p\xi}} & L_{q_{pu}} & L_{q_{pv}} & L_{q_{pw}} & L_{q_{pp}} \end{bmatrix}$$

with the sub-operators given by

$$\begin{aligned}
&L_{q_{\xi\xi}} = -U_0\partial_x, L_{q_{\xi u}} = \xi_0\partial_x, L_{q_{\xi v}} = \xi_0\partial_y - \xi_0', L_{q_{\xi w}} = \xi_0\partial_z, L_{q_{\xi p}} = 0,\\
&L_{q_{u\xi}} = \frac{\xi_0}{Re}(\eta_1 + \eta_2\partial_y), L_{q_{uu}} = -U_0\partial_x + \frac{\xi_0}{Re}\left(\eta_0\left(\nabla^2 + \frac{1}{3}\partial_{xx}\right) + \eta_0'\partial_y\right), L_{q_{uv}} = -U_0' + \frac{\xi_0}{Re}\left(\frac{1}{3}\eta_0\partial_{xy} + \eta_0'\partial_x\right),\\
&L_{q_{uw}} = \frac{\xi_0\eta_0}{3Re}\partial_{xz}, L_{q_{up}} = -\frac{1}{\gamma M_r^2}\xi_0\partial_x + \frac{\xi_0}{Re}\left(\eta_1\xi_0 + \eta_2\xi_0' + \eta_2\xi_0\partial_y\right), L_{q_{v\xi}} = \frac{\xi_0}{Re}\eta_{T_0}U_0'\partial_x,\\
&L_{q_{vu}} = \frac{\xi_0}{Re}\left(\frac{1}{3}\eta_0\partial_{xy} - \frac{2}{3}\eta_0'\partial_x\right), L_{q_{vv}} = -U_0\partial_x + \frac{\xi_0}{Re}\left(\eta_0\left(\nabla^2 + \frac{1}{3}\partial_{yy}\right) + \frac{4}{3}\eta_0'\partial_y\right), L_{q_{vw}} = \frac{\xi_0}{Re}\left(\frac{1}{3}\eta_0\partial_{yz} - \frac{2}{3}\eta_0'\partial_z\right),\\
&L_{q_{vp}} = -\frac{1}{\gamma M_r^2}\xi_0\partial_y + \frac{\xi_0}{Re}\eta_{T_0}U_0'\xi_0\partial_x, L_{q_{w\xi}} = 0, L_{q_{wu}} = \frac{\xi_0\eta_0}{3Re}\partial_{xz}, L_{q_{wv}} = \frac{\xi_0}{Re}\left(\frac{1}{3}\eta_0\partial_{yz} + \eta_0'\partial_z\right),\\
&L_{q_{ww}} = -U_0\partial_x + \frac{\xi_0}{Re}\left(\eta_0\left(\nabla^2 + \frac{1}{3}\partial_{zz}\right) + \eta_0'\partial_y\right), L_{q_{wp}} = -\frac{1}{\gamma M_r^2}\xi_0\partial_z,\\
&L_{q_{p\xi}} = \frac{\gamma(\gamma-1)M_r^2}{Re}\eta_{T_0}(U_0')^2 + \frac{\gamma}{RePr}\left(\eta_0\nabla^2 + \eta_0'\partial_y + \eta_3 + \eta_{T_0}\xi_0'\partial_y\right), L_{q_{pu}} = -\gamma\partial_x + \frac{\gamma(\gamma-1)M_r^2}{Re}\left(2\eta_0U_0'\partial_y\right),
\end{aligned} \tag{9}$$

$$L_{q_{pv}} = -\gamma\partial_y + \frac{\gamma(\gamma-1)M_r^2}{Re}\left(2\eta_0 U_0'\partial_x\right), L_{q_{pw}} = -\gamma\partial_z,$$
$$L_{q_{pp}} = -U_0\partial_x + \frac{\gamma(\gamma-1)M_r^2}{Re}\eta_{T_0}(U_0')^2\xi_0 + \frac{\gamma}{RePr}\left(\eta_0\xi_0\nabla^2 + 2\eta_0\xi_0'\partial_y + \eta_0\xi_0'' + \eta_0'\left(\xi_0' + \xi_0\partial_y\right) + \eta_3\xi_0 + \eta_{T_0}\xi_0\xi_0'\partial_y + \eta_{T_0}(\xi_0')^2\right)$$

where

$$\eta_1 = \eta_{TT_0}T_0'U_0' + \eta_{T_0}U_0''$$
$$\eta_2 = \eta_{T_0}U_0'$$
$$\eta_3 = \eta_{T_0}T_0'' + \eta_{TT_0}(T_0')^2.$$

C. Chu Energy Expression for the Quadratic+ Formulation

Chu energy [16] has been extensively utilized for the inner product in resolvent analysis of compressible flows [1, 5, 6]. The expression of Chu energy in terms of the Cubic+ variables ($\mathbf{q}_c$) is well known [17]. Here, we derive an expression for the Chu energy in terms of the variables used in Quadratic+ formulation ($\mathbf{q}_q$) based on the principles outlined in Ref. [14]. We start by defining the nonlinear transformation between $\mathbf{q}_c$ and $\mathbf{q}_q$ as

$$\mathbf{q}_c = (\rho, u, v, w, T) = (\frac{1}{\xi}, u, v, w, p\xi) = g(\xi, u, v, w, p) = g(\mathbf{q}_q)$$

We need the expression of the Jacobian of $g(\cdot)$ with respect to $\mathbf{q}_q$, which is given by

$$\partial_{\mathbf{q}_q} g = \begin{bmatrix} -\frac{1}{\xi^2} & 0 & 0 & 0 & 0 \\ 0 & 1 & 0 & 0 & 0 \\ 0 & 0 & 1 & 0 & 0 \\ 0 & 0 & 0 & 1 & 0 \\ p & 0 & 0 & 0 & \xi \end{bmatrix}.$$

Let the Chu energy expressions in terms of $\mathbf{q}_c$ and $\mathbf{q}_q$ be denoted by $\mathcal{E}_c$ and $\mathcal{E}_q$, respectively, with $\mathcal{E}_c$ given by [17]

$$\mathcal{E}_c = \text{diag}\left(\frac{T_0}{\rho_0\gamma M_r^2}, \rho_0, \rho_0, \rho_0, \frac{\rho_0}{\gamma(\gamma-1)M_r^2 T_0}\right).$$

The equivalent expression for $\mathcal{E}_q$ is then given by

$$\mathcal{E}_q = \left(\partial_{\mathbf{q}_q} g\big|_{\mathbf{q}_q=\mathbf{q}_{q_0}}\right)^* \mathcal{E}_c \left(\partial_{\mathbf{q}_q} g\big|_{\mathbf{q}_q=\mathbf{q}_{q_0}}\right)$$

where $(\cdot)^*$ stands for Hermitian transpose, while $\mathbf{q}_{q_0}$ denotes the base flow described in terms of $\mathbf{q}_q$. Carrying out these calculations leads to the following expression:

$$\mathcal{E}_q = \begin{bmatrix} \frac{T_0}{\xi_0^3\gamma M_r^2} + \frac{p_0^2\rho_0}{\gamma(\gamma-1)M_r^2 T_0} & 0 & 0 & 0 & \frac{p_0}{\gamma(\gamma-1)M_r^2 T_0} \\ 0 & \rho_0 & 0 & 0 & 0 \\ 0 & 0 & \rho_0 & 0 & 0 \\ 0 & 0 & 0 & \rho_0 & 0 \\ \frac{p_0}{\gamma(\gamma-1)M_r^2 T_0} & 0 & 0 & 0 & \frac{\xi_0}{\gamma(\gamma-1)M_r^2 T_0} \end{bmatrix}.$$

III. Resolvent Analysis: Compressible Plane Couette Flow

In this section, we provide an overview of the resolvent analysis and discuss results pertaining to compressible plane Couette flow. This flow provides a convenient canonical setup for investigating compressible flows and has been

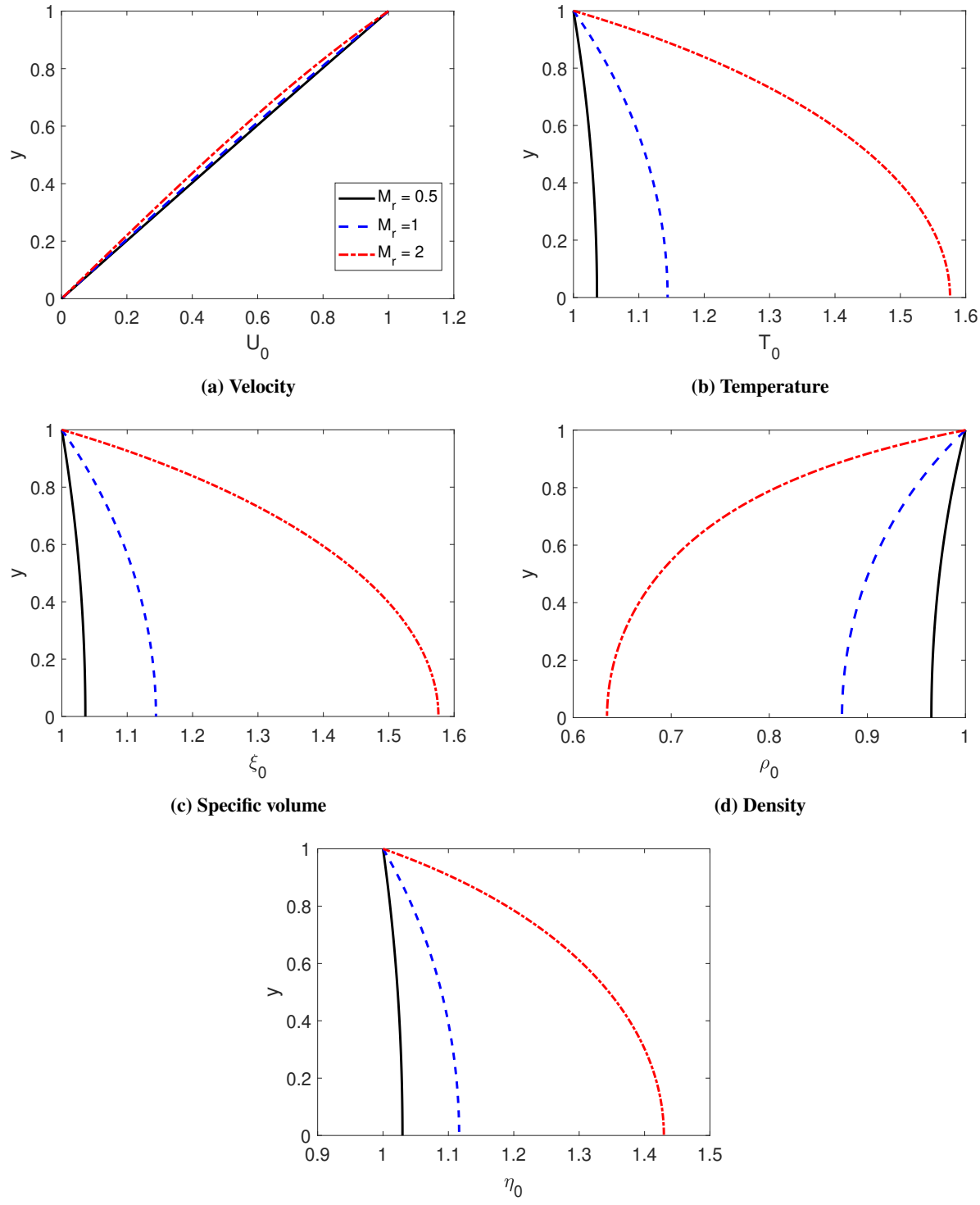

(a) Velocity

(b) Temperature

(c) Specific volume

(d) Density

(e) Viscosity coefficient

Fig. 2 Steady base flow profiles of compressible plane Couette flow for different Mach numbers.

utilized quite extensively in the literature [5, 15, 18–20]. The base flow profiles for this flow can be computed relatively easily (see, for example, Refs. [5, 9] for details). Sample base flow profiles for different Mach numbers are shown in

Fig. 2. We utilize a Fourier-Chebyshev-Fourier spectral discretization for the perturbation equations, i.e., we assume solutions of the form $\mathbf{q}_i(x, y, z, t) = \hat{\mathbf{q}}_i(y) \exp(\mathbf{i}(k_x x + k_z z - \omega t))$ where $\mathbf{i} = \sqrt{-1}$ is the imaginary unit, $i = c, q$ is used to designate the formulations ($i = c$ for Cubic+ and $i = q$ for Quadratic+), and ω, k_x and k_z are the temporal frequency, streamwise wavenumber and spanwise wavenumber, respectively. The discretized versions of the perturbation dynamics (5) and (8) can be expressed as

$$\hat{\mathbf{q}}_i = \left(-\mathbf{i}\omega\mathbf{I} - \hat{\mathbf{L}}_i(k_x, k_z)\right)^{-1} \hat{\mathbf{f}}_i$$

where $\mathcal{R}_i(k_x, k_z, \omega) = \left(-\mathbf{i}\omega\mathbf{I} - \hat{\mathbf{L}}_i(k_x, k_z)\right)^{-1} \in \mathbb{C}^{n\times n}$ are the associated resolvent operators. Here, we have $n = 5N_y$ where N_y denotes the number of Chebyshev collocation points in the wall-normal direction. Expressions for the discretized linear operators $\hat{\mathbf{L}}_i$ are provided in Appendix A. Resolvent analysis focuses on the maximum singular value and the associated singular vectors of this operator [5, 10, 11]. In the subsequent discussions, we utilize the following two notions of the resolvent gain:

$$\begin{aligned} \sigma_{\mathcal{R}_i}(k_x, k_z, \omega) &= \bar{\sigma}\left(\mathcal{R}_i(k_x, k_z, \omega)\right), \\ \sigma_{\mathcal{R}_i}(k_x, k_z) &= \sup_{\omega\in\mathbb{R}} \bar{\sigma}\left(\mathcal{R}_i(k_x, k_z, \omega)\right) \end{aligned} \tag{10}$$

where $\bar{\sigma}(\mathbf{M})$ denotes the largest singular value of a matrix $\mathbf{M}$. A system-theoretic interpretation of $\sigma_{\mathcal{R}_i}(k_x, k_z)$–which are the H_∞ norm of the associated linear perturbation dynamics–is that these provide the worst-case (i.e., largest) gain induced by the nonlinear forcing terms $\hat{\mathbf{f}}_i$ on the perturbed flow variables $\hat{\mathbf{q}}_i$. Note that computation of $\sigma_{\mathcal{R}_i}(k_x, k_z)$ essentially boils down to computing the maximum of $\sigma_{\mathcal{R}_i}(k_x, k_z, \omega)$ over an appropriate grid of $\omega \in \mathbb{R}$.

A. Code Validation

According to the discussion in Section 2.1 in Ref. [14], the discretized linear operators $\hat{\mathbf{L}}_i$ associated with the two formulations discussed here are guaranteed to share the same eigenvalues because of the steady base flow. The eigenvalue spectra obtained through our numerical implementation are shown in Fig. 3. These results demonstrate that the eigenvalues for two formulations match closely, as theoretically expected. The 'Y' shape of the eigenvalues in Fig. 3b are consistent with the existing literature [5, 18, 19]. Note that these eigenvalues are associated with the viscous eigenmodes, i.e., modes that arise due to the viscous terms in the momentum and energy equations [18]. In addition, the shape/pattern of the eigenvalues depicted in Fig. 3a away from the imaginary axis is also expected (see, for example, similar trends reported in Ref. [19]). These eigenvalues belong to the inviscid or acoustic eigenmodes [5, 18, 19].

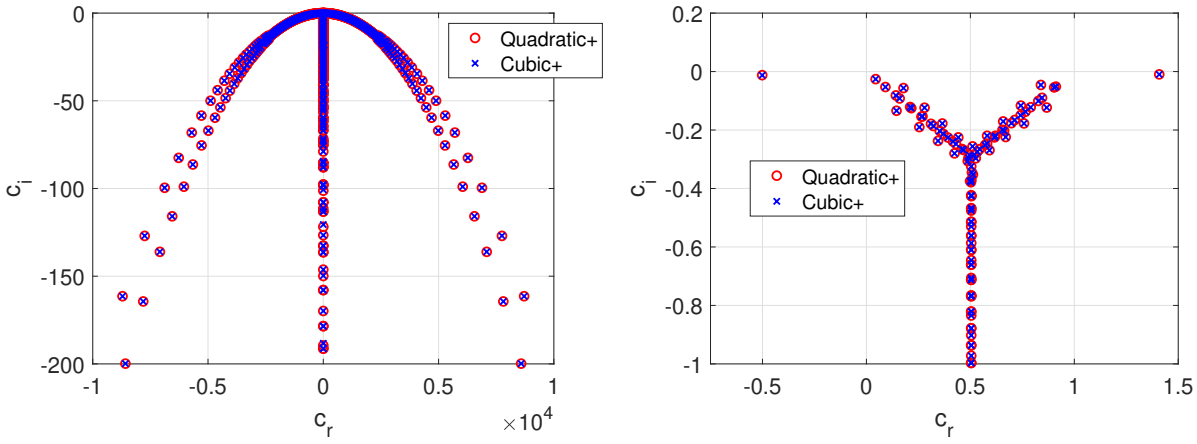

Fig. 3 Eigenvalue spectra of the linear operators for $k_x = k_z = 0.1$, $Re = 2 \times 10^5$, $M_r = 2$, $Pr = 0.72$, $N_y = 200$. The eigenvalues are plotted in terms of complex wavespeeds $c_w = c_r + \mathbf{i}c_i = \omega_i/k_x$ where ω_i satisfies $\hat{\mathbf{L}}_i(k_x, k_z)\mathbf{q}_i = -i\omega_i\mathbf{q}_i$ for $i = q, c$. The two sets of eigenvalues match up, which is expected due to the steadiness of the base flow, as discussed in Ref. [14].

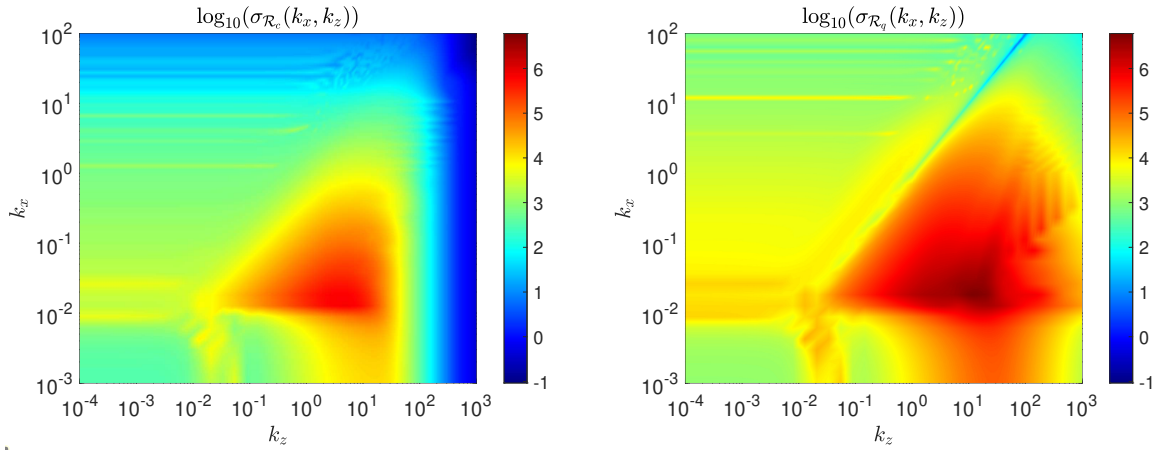

(a) $M_r = 2$

(b) $M_r = 2$

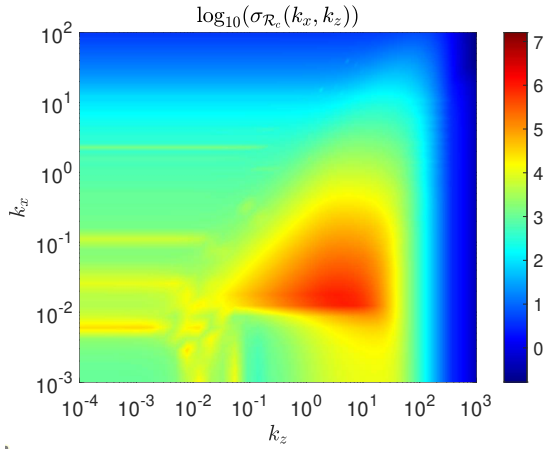

(c) $M_r = 1$

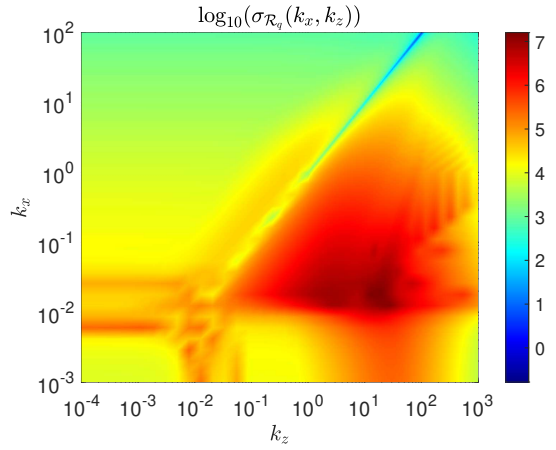

(d) $M_r = 1$

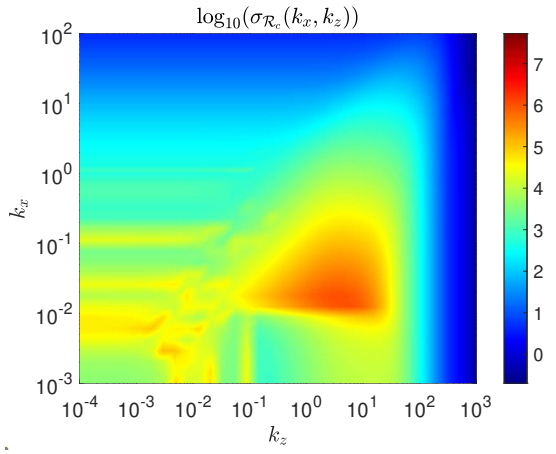

(e) $M_r = 0.5$

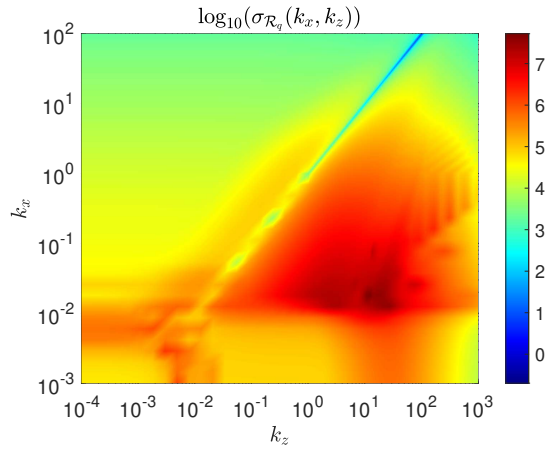

(f) $M_r = 0.5$

Fig. 4 The log-scaled values of resolvent gains $\sigma_{\mathcal{R}_i}(k_x, k_z)$ over the wavenumber pair grid for $Re = 2 \times 10^5$, $Pr = 0.72$, $N_y = 200$. Note that the Chu energy is utilized for the compressible inner product. Despite the qualitative similarities overall, the Quadratic+ formulation predicts larger hotspots and features localized oblique regions of high gain.

B. Resolvent Gain Variation in the Wavenumber Space

To study the variation of the resolvent gains $\sigma_{\mathcal{R}_i}(k_x, k_z)$ over the wavenumber pairs, we choose a 60×80 grid of $k_x \times k_z$ with logarithmically spaced values of $k_x \in [10^{-3}, 10^2]$ and $k_z \in [10^{-4}, 10^3]$. The temporal frequency grid comprises of 50 logarithmically spaced points between -10 and 10, i.e., $\omega \in [-10, 10]$. The results for three different Mach numbers are shown in Fig. 4. A closer inspection of the results reveals that the Cubic+ formulation predicts lower amplifications than the Quadratic+ formulation at more than 99.5% of all (k_x, k_z) grid points for each of the three Mach numbers considered here. The hotspots in the Quadratic+ results are also much larger compared to the hotspots in the other set of results. There are oblique waves/structures of relatively larger gains approximately for $k_x \in (10^{-1}, 10)$, $k_z \in (10^{-2}, 10)$ in the Quadratic+ results for all three Mach numbers. These, however, are absent in the Cubic+ results. While it is possible that these oblique structures signify some mechanisms of instability, it is also possible that these do not represent the actual flow physics and that the Cubic+ results indeed capture the true system behavior. In terms of similarities, both formulations predict several horizontal bands of high gains for wavenumbers in the region $k_x \in (10^{-2.5}, 10^{-1})$, $k_z \in (10^{-4}, 10^{-1})$. These potential mechanisms of instability are dependent on the Mach number as these high-gain bands start to disappear as the Mach number increases. At a large fraction of the wavenumber pairs on the grid in Fig. 4, the resolvent gains decrease with an an increase in the Mach number for both the formulations-more so in the Quadratic+ results. This is consistent with the results reported in Ref. [5]. Also, as remarked by the authors in [5], this variation with Mach number is also consistent with the results reported on transient energy growth for the compressible Couette flow [15, 19].

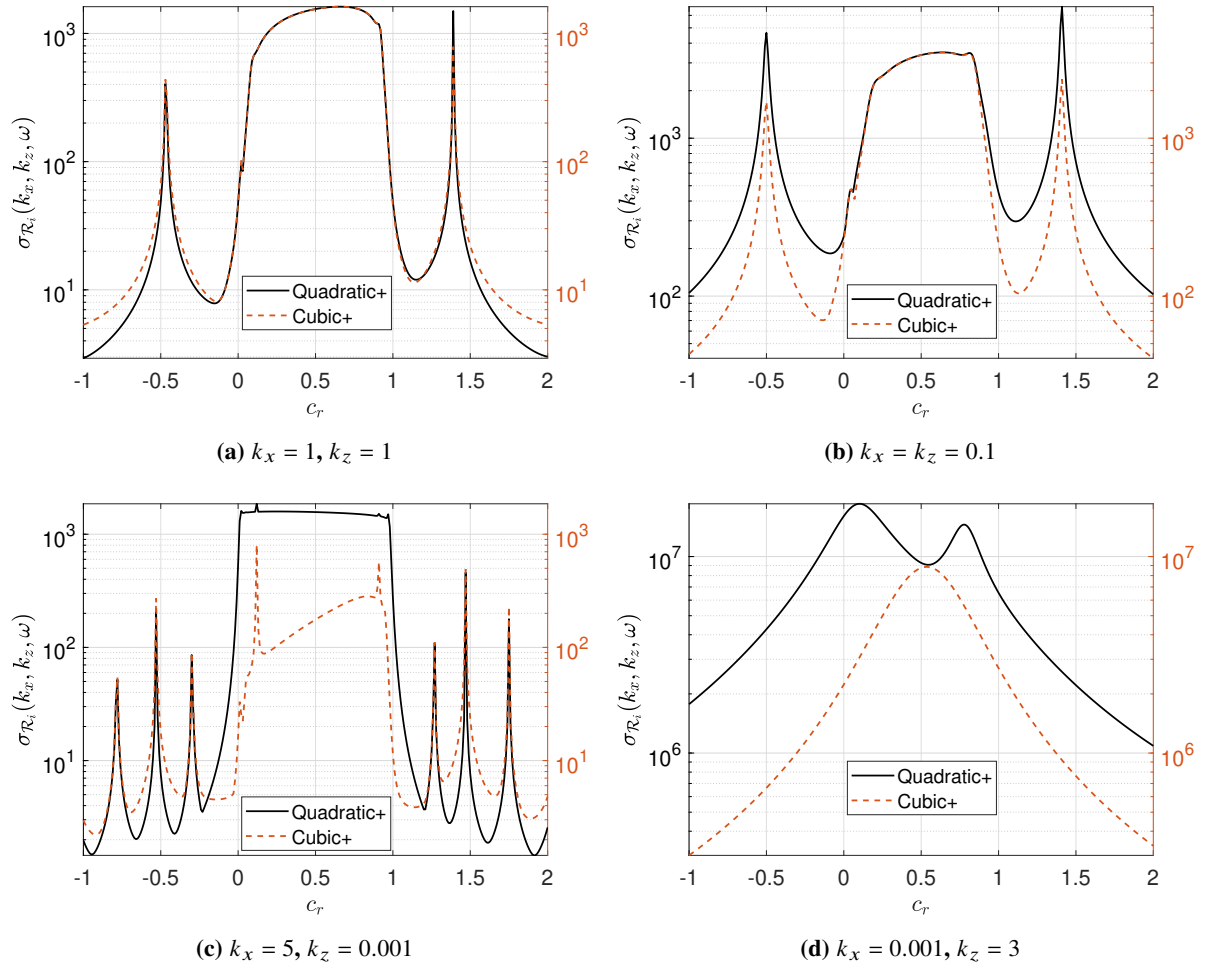

(a) $k_x = 1$, $k_z = 1$

(b) $k_x = k_z = 0.1$

(c) $k_x = 5$, $k_z = 0.001$

(d) $k_x = 0.001$, $k_z = 3$

Fig. 5 The resolvent gains $\sigma_{\mathcal{R}_i}(k_x, k_z, \omega)$ as functions of c_r for $Re = 2 \times 10^5$, $M_r = 2$, $Pr = 0.72$, $N_y = 200$. Note that the variation in c_r for a fixed k_x means variation in ω since $\omega = k_x c_r$. The Chu energy is used for the compressible inner products. The results are qualitatively similar in (a), (b) but start to differ more in (c), (d).

C. Temporal Behavior of Resolvent Gains at Fixed Wavenumber Pairs

The variations of the resolvent gains with the temporal frequency are depicted in Fig. 5 at four different wavenumber pairs. As mentioned earlier, the peak values in the Quadratic+ results are higher overall compared to the ones in the Cubic+ results. The patterns of variations are qualitatively similar for wavenumber pairs with similar values of k_x and k_z (i.e., potentially representing oblique structures, see Figs. 5a, 5b). However, as shown in Figs. 5d, 5c, the variations in the gains start to differ if either k_x or k_z is significantly different from the other. Upon a closer inspection of the result in Fig. 5b, the largest value in $\sigma_{\mathcal{R}_c}(k_x, k_z, \omega)$ occurs approximately at $c_r = 0.82$, whereas the largest in $\sigma_{\mathcal{R}_q}(k_x, k_z, \omega)$ corresponds to the peak approximately at $c_r = 1.41$. Therefore, not only are the magnitudes of amplification predicted by the two formulations different, but also the estimated temporal frequencies for largest amplification are different across these two formulations. Moreover, the results shown in Figs. 5c, 5d indicate drastically different predictions by the two formulations. In Fig. 5c, although both the formulations feature two distinct peaks at $c_r \approx 0$ and $c_r \approx 1$, the local behavior of the gains are quite different for $c_r \in (0, 1)$. Finally in Fig. 5d, while $\sigma_{\mathcal{R}_c}(k_x, k_z, \omega)$ showcases a single global peak, $\sigma_{\mathcal{R}_q}(k_x, k_z, \omega)$ features two distinct peaks with a local minimum (at $c_r \approx 0.55$) that approximately coincides with the global peak in $\sigma_{\mathcal{R}_c}(k_x, k_z, \omega)$. Sample results for the resolvent response mode shapes–obtained from

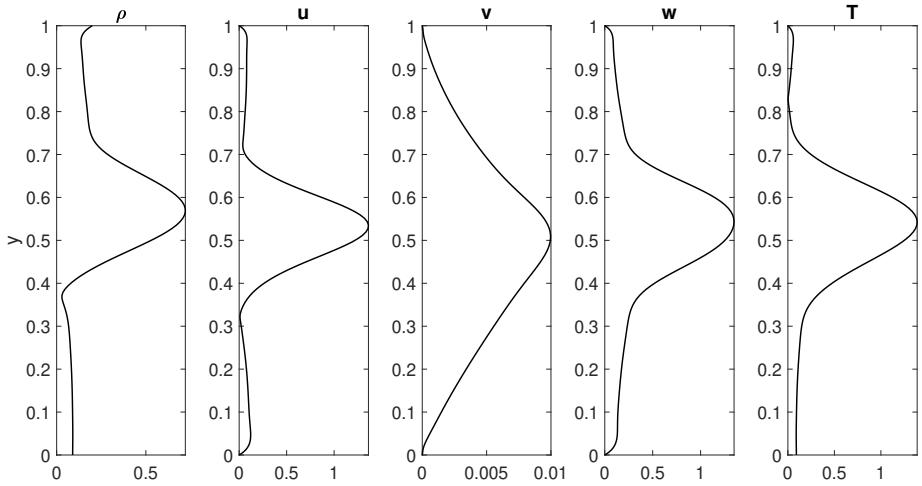

(a) Cubic+ formulation

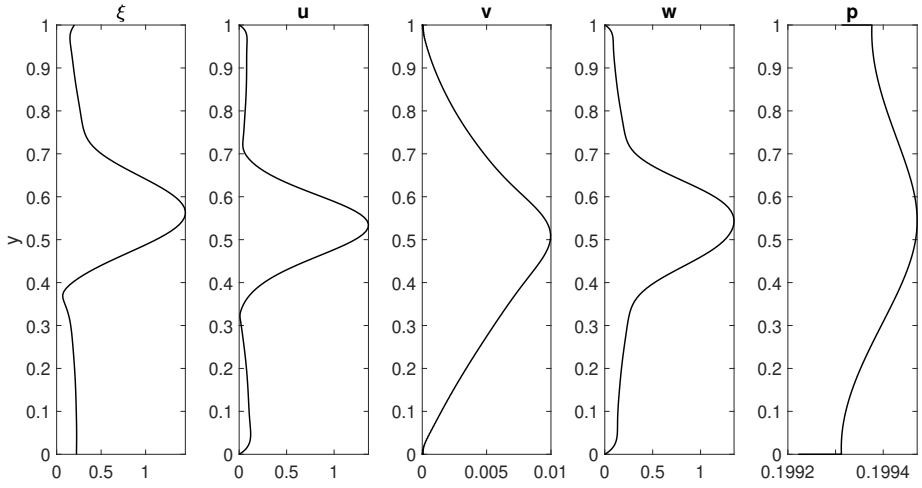

(b) Quadratic+ formulation

Fig. 6 The response mode shapes (absolute values) corresponding to both the formulations for $k_x = k_z = 0.1$ and $c_r = 0.5$. The Chu energy is used for the compressible inner product.

the left singular vectors associated with $\sigma_{\mathcal{R}_i}(k_x, k_z, \omega)$ (see Eq. (10))–for both the formulations are shown in Fig. 6. The velocity mode shapes appear to be similar across the two sets of results. Our future work will focus on studying the resolvent modes in more detail.

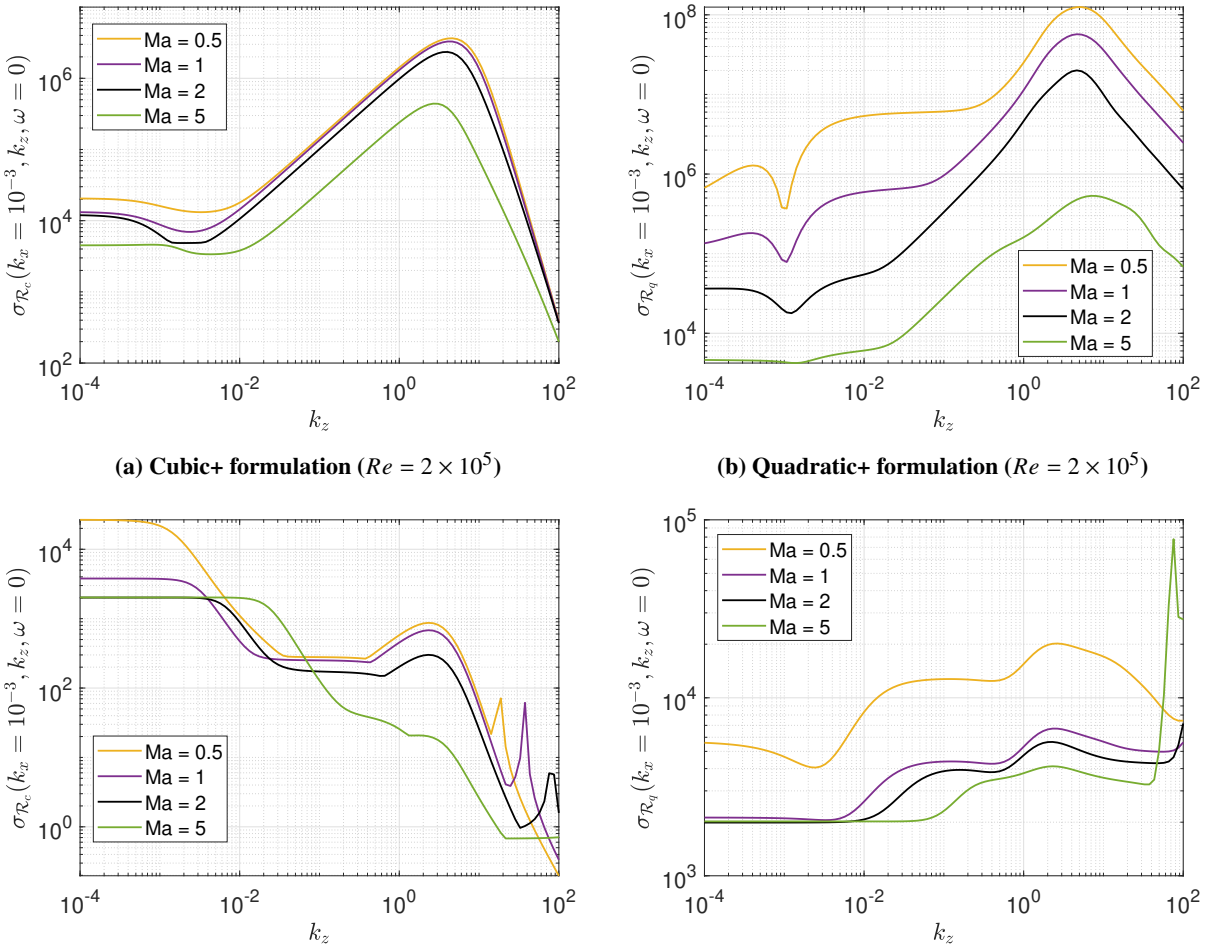

(a) Cubic+ formulation ($Re = 2 \times 10^5$)

(b) Quadratic+ formulation ($Re = 2 \times 10^5$)

(c) Cubic+ formulation ($Re = 10^3$)

(d) Quadratic+ formulation ($Re = 10^3$)

Fig. 7 The resolvent gains $\sigma_{\mathcal{R}_i}(k_x, k_z, \omega)$ as functions of k_z for $k_x = 0.001$, $\omega = 0$. Results are shown for four different Mach numbers and two different Reynolds numbers. While there are qualitative similarities between the two sets of results for $Re = 2 \times 10^5$, the implications are quite different for $Re = 10^3$.

D. Effects of Mach Number and Reynolds Number

Next, we study the effects of varying the Mach number and Reynolds number on the resolvent gain $\sigma_{\mathcal{R}_i}(k_x, k_z, \omega)$ in a manner similar to the analysis done in Ref. [5]. Therefore, we fix the values of k_x and ω, and focus on the variation of the resolvent gain over a grid of k_z values for different Mach numbers and Reynolds numbers. The results of this analysis are shown in Fig. 7, where we have utilized a 100-point grid of k_z with logarithmically spaced points between 10^{-4} and 10^2. Similar to the observations made in [5], the Cubic+ results feature localized peaks for $k_z \approx (3, 5)$ across the different Mach numbers considered for $Re = 2 \times 10^5$ (see Fig. 7a). As shown in Fig. 7b, the Quadratic+ results indicate a similar trend as well. Overall, the two sets of results for $Re = 2 \times 10^5$ are qualitatively similar but that is not the case for $Re = 10^3$, as depicted in Figs. 7c, 7d. While the Cubic+ results suggest a significant overall reduction in the gains as k_z increases, the Quadratic+ results show a slight increase in the gains as k_z increases, which is true for all Mach numbers except $M_r = 5$. For $M_r = 5$, there is a sharp spike in the gain at $k_z \approx 43$.

E. Choice of Energy Norm for Compressible Inner Product

Finally, we study the effects of the energy norm/expression utilized in the compressible inner product. To highlight the differences brought about solely by the energy norm used, we recompute the results provided in Fig. 5 with the Chu energy replaced by the kinetic energy for the inner product. The results we obtained are shown in Fig. 8. It is noteworthy that the Cubic+ formulation now predicts higher resolvent gains at almost all temporal frequencies (i.e., c_r values) depicted in Fig. 8. It is also interesting that the qualitative behavior of the gains do not alter significantly when k_x and k_z are equal (compare Figs. 5a, 5b with 8a, 8b). Furthermore, the discrepancies highlighted in Fig. 5d persists even when kinetic energy (a semi-norm) is utilized in the inner product definition (compare Figs. 5d and 8d).

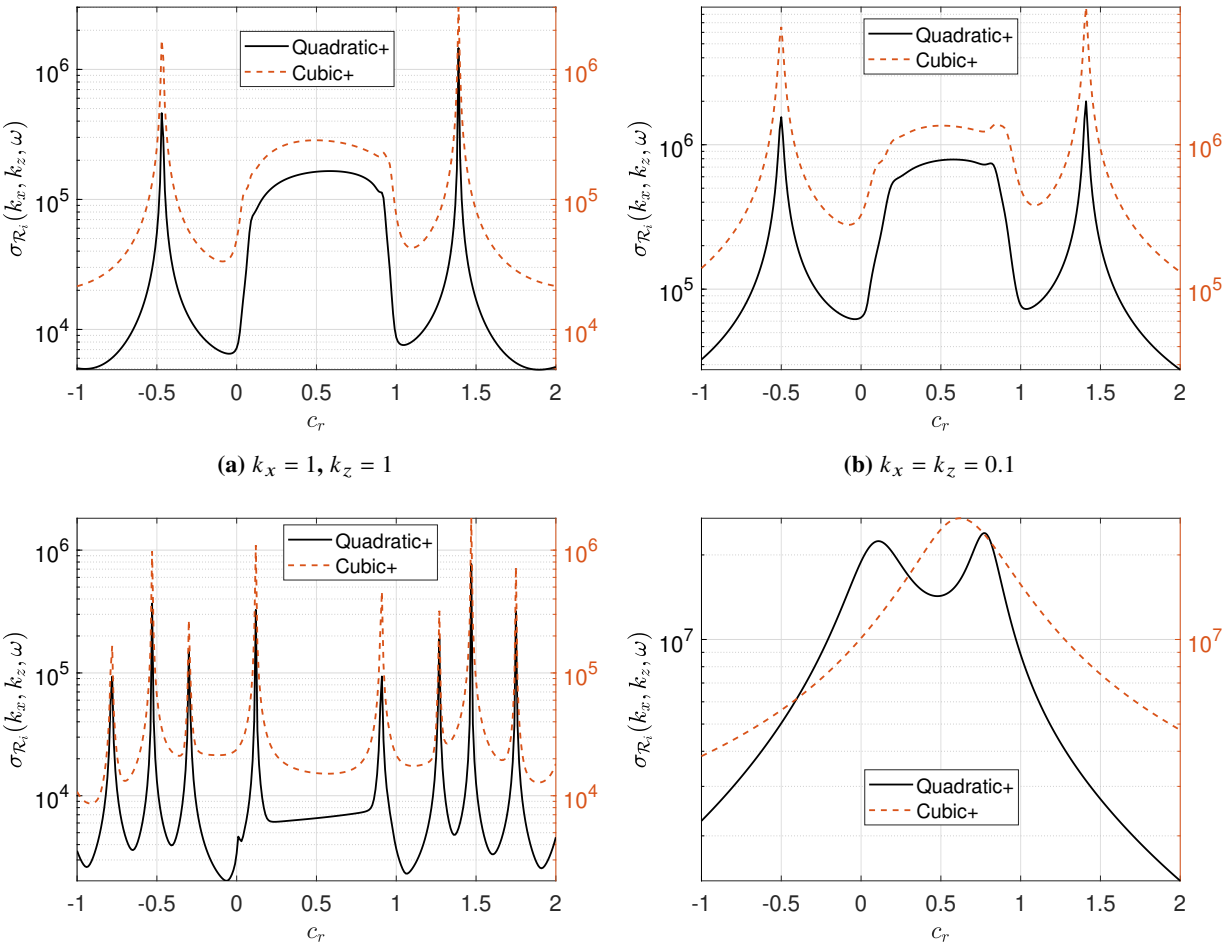

(a) $k_x = 1$, $k_z = 1$ **(b)** $k_x = k_z = 0.1$

(c) $k_x = 5$, $k_z = 0.001$ **(d)** $k_x = 0.001$, $k_z = 3$

Fig. 8 The resolvent gains $\sigma_{\mathcal{R}_i}(k_x, k_z, \omega)$ as functions of c_r for $Re = 2 \times 10^5$, $M_r = 2$, $Pr = 0.72$, $N_y = 200$. These results are a re-computation of the results showcased in Fig. 5 with kinetic energy replacing the Chu energy for the compressible inner products. Therefore, any differences with the equivalent plots in Fig. 5 are solely due to the choice of energy norm.

IV. Conclusions

In this paper, we exploited the non-unique nature of resolvent analysis–that arises if different sets of variables, even when related via some nonlinear transformations, are used to describe a given flow [14]–to reveal conflicting predictions and discrepancies regarding instability mechanisms associated with a compressible plane Couette flow. Two resolvent formulations are implemented and the results are compared over a broad range of Mach numbers, which indicate substantially different temporal behaviors of the linearized flow dynamics at some values of the streamwise and

spanwise wavenumbers. It is, therefore, crucial to substantiate these contradictory observations through high-fidelity numerical simulations and/or experimental studies in the future. While the study here focused on the resolvent gain (with two variations studied), our future work will involve investigating the resolvent mode shapes provided by the two formulations. Furthermore, we will implement these formulations to study turbulent wall-bounded flows going forward.

Acknowledgments

This material is based upon work supported by the Air Force Office of Scientific Research under award number FA9550-21-1-0106, the Army Research Office under award number W911NF-20-1-0156, the National Science Foundation under award number CBET-1943988, and the Office of Naval Research under award number N00014-22-1-2029. The authors acknowledge the Minnesota Supercomputing Institute (MSI) at the University of Minnesota for providing the computational resources utilized to generate some of the numerical results. The authors thank Prof. Scott Dawson for sharing his code for the Cubic+ formulation.

References

[1] Bae, H. J., Dawson, S. T. M., and McKeon, B. J., "Resolvent-based study of compressibility effects on supersonic turbulent boundary layers," *Journal of Fluid Mechanics*, 2019.

[2] Chen, X., Cheng, C., Fu, L., and Gan, J., "Linear response analysis of supersonic turbulent channel flows with a large parameter space," *Journal of Fluid Mechanics*, Vol. 962, 2023, p. A7.

[3] Jovanović, M. R., and Bamieh, B., "Componentwise energy amplification in channel flows," *Journal of Fluid Mechanics*, Vol. 534, 2005, pp. 145–183.

[4] McKeon, B. J., and Sharma, A. S., "A critical-layer framework for turbulent pipe flow," *Journal of Fluid Mechanics*, 2010.

[5] Dawson, S. T. M., and McKeon, B. J., "Studying the effects of compressibility in planar Couette flow using resolvent analysis," *AIAA Paper 2019-2139*, 2019.

[6] Bae, H. J., Dawson, S. T., and McKeon, B. J., "Studying the effect of wall cooling in supersonic boundary layer flow using resolvent analysis," *AIAA Paper 2020-0575*, 2020.

[7] Dwivedi, A., Sidharth, G., Nichols, J. W., Candler, G. V., and Jovanović, M. R., "Reattachment streaks in hypersonic compression ramp flow: an input–output analysis," *Journal of Fluid Mechanics*, Vol. 880, 2019, pp. 113–135.

[8] Nichols, J. W., and Candler, G. V., "Input-output analysis of complex hypersonic boundary layers," *AIAA Scitech 2019 Forum*, 2019, p. 1383.

[9] Bhattacharjee, D., Mushtaq, T., Seiler, P. J., and Hemati, M., "Structured Input-Output Analysis of Compressible Plane Couette Flow," *AIAA SCITECH 2023 Forum*, 2023, p. 1984.

[10] McKeon, B. J., and Sharma, A. S., "A critical-layer framework for turbulent pipe flow," *Journal of Fluid Mechanics*, Vol. 658, 2010, pp. 336–382.

[11] McKeon, B., "The engine behind (wall) turbulence: perspectives on scale interactions," *Journal of Fluid Mechanics*, Vol. 817, 2017, p. P1.

[12] Liu, C., and Gayme, D. F., "Structured input–output analysis of transitional wall-bounded flows," *Journal of Fluid Mechanics*, Vol. 927, 2021.

[13] Packard, A., and Doyle, J., "The complex structured singular value," *Automatica*, Vol. 29, No. 1, 1993, pp. 71–109.

[14] Karban, U., Bugeat, B., Martini, E., Towne, A., Cavalieri, A., Lesshafft, L., Agarwal, A., Jordan, P., and Colonius, T., "Ambiguity in mean-flow-based linear analysis," *Journal of Fluid Mechanics*, Vol. 900, 2020, p. R5.

[15] Malik, M., Dey, J., and Alam, M., "Linear stability, transient energy growth, and the role of viscosity stratification in compressible plane Couette flow," *Physical Review E*, Vol. 77, No. 3, 2008, p. 036322.

[16] Chu, B.-T., "On the energy transfer to small disturbances in fluid flow (Part I)," *Acta Mechanica*, Vol. 1, No. 3, 1965, pp. 215–234.

[17] Hanifi, A., Schmid, P. J., and Henningson, D. S., "Transient growth in compressible boundary layer flow," *Physics of Fluids*, Vol. 8, No. 3, 1996, pp. 826–837.

[18] Duck, P. W., Erlebacher, G., and Hussaini, M. Y., "On the linear stability of compressible plane Couette flow," *Journal of Fluid Mechanics*, Vol. 258, 1994.

[19] Malik, M., Alam, M., and Dey, J., "Nonmodal energy growth and optimal perturbations in compressible plane Couette flow," *Physics of Fluids*, Vol. 18, No. 3, 2006.

[20] Hu, S., and Zhong, Z., "Linear stability of viscous supersonic plane Couette flow," *Physics of Fluids*, Vol. 10, No. 709, 1998.

A. Details of the Discretized Linear Operators

Discretization of the linear operators require an expansion using Chebyshev polynomials in the wall-normal direction and Fourier modes in the streamwise and spanwise directions. The resulting discretized sub-operators (see (6) and (9) for the continuous forms) for both the formulations are summarized in the following where D_y and D_{yy} denote the first and second derivatives in the wall-normal direction.

A. Cubic+ formulation

$$
\begin{aligned}
\hat{L}_{c_{\rho\rho}} &= -\mathbf{i}k_x U_0 \\
\hat{L}_{c_{\rho u}} &= -\mathbf{i}k_x \rho_0 \\
\hat{L}_{c_{\rho v}} &= -\rho_0' - \rho_0 D_y \\
\hat{L}_{c_{\rho w}} &= -\mathbf{i}k_z \rho_0 \\
\hat{L}_{c_{\rho T}} &= 0 \\
\hat{L}_{c_{u\rho}} &= -\mathbf{i}k_x \frac{1}{\gamma M_r^2} T_0^2 \\
\hat{L}_{c_{uu}} &= -\mathbf{i}k_x U_0 - \frac{T_0}{Re}\left[\eta_0\left(\frac{4}{3}k_x^2 - D_{yy} + k_z^2\right) - \eta_0' D_y\right] \\
\hat{L}_{c_{uv}} &= -U_0' + \mathbf{i}k_x \frac{T_0}{3Re}\left[\eta_0 D_y + 3\eta_0'\right] \\
\hat{L}_{c_{uw}} &= -k_x k_z \frac{T_0 \eta_0}{3Re} \\
\hat{L}_{c_{uT}} &= -\mathbf{i}k_x \frac{1}{\gamma M_r^2} + \frac{T_0}{Re}\left(\eta_{TT_0} T_0' U_0' + \eta_{T_0} U_0' D_y + \eta_{T_0} U_0''\right) \\
\hat{L}_{c_{v\rho}} &= -\frac{T_0}{\gamma M_r^2}\left(T_0 D_y + T_0'\right) \\
\hat{L}_{c_{vu}} &= \mathbf{i}k_x \frac{T_0}{3Re}\left[\eta_0 D_y - 2\eta_0'\right] \\
\hat{L}_{c_{vv}} &= -\mathbf{i}k_x U_0 - \frac{T_0}{Re}\left[\eta_0\left(k_x^2 - \frac{4}{3}D_{yy} + k_z^2\right) - \frac{4}{3}\eta_0' D_y\right] \\
\hat{L}_{c_{vw}} &= \mathbf{i}k_z \frac{T_0}{3Re}\left[\eta_0 D_y - 2\eta_0'\right] \\
\hat{L}_{c_{vT}} &= -\frac{1}{\gamma M_r^2}\left(T_0 \rho_0' + D_y\right) + \mathbf{i}k_x \frac{T_0}{Re}\left(\eta_{T_0} U_0'\right) \\
\hat{L}_{c_{w\rho}} &= -\mathbf{i}k_z \frac{T_0^2}{\gamma M_r^2} \\
\hat{L}_{c_{wu}} &= -k_x k_z \frac{T_0 \eta_0}{3Re} \\
\hat{L}_{c_{wv}} &= \mathbf{i}k_z \frac{T_0}{3Re}\left[\eta_0 D_y + 3\eta_0'\right]
\end{aligned}
$$

$$\hat{L}_{c_{ww}} = -\mathbf{i}k_x U_0 - \frac{T_0}{Re}\left[\eta_0\left(k_x^2 - D_{yy} + \frac{4}{3}k_z^2\right) - \eta_0' D_y\right]$$
$$\hat{L}_{c_{wT}} = -\mathbf{i}k_z \frac{1}{\gamma M_r^2}$$
$$\hat{L}_{c_{T\rho}} = 0$$
$$\hat{L}_{c_{Tu}} = \mathbf{i}k_x T_0(1-\gamma) + \frac{T_0\gamma(\gamma-1)M_r^2}{Re}\left(2\eta_0 U_0'\right) D_y$$
$$\hat{L}_{c_{Tv}} = -T_0' + T_0(1-\gamma)D_y + \mathbf{i}k_x \frac{T_0\gamma(\gamma-1)M_r^2}{Re}\left(2\eta_0 U_0'\right)$$
$$\hat{L}_{c_{Tw}} = \mathbf{i}k_z T_0(1-\gamma)$$
$$\hat{L}_{c_{TT}} = -\mathbf{i}k_x U_0 + \frac{T_0\gamma(\gamma-1)M_r^2}{Re}\eta_{T_0}(U_0')^2 + \frac{T_0\gamma}{RePr}\left(\eta_{T_0}T_0'' + \eta_{TT_0}(T_0')^2 + 2\eta_0' D_y + \eta_0(-k_x^2 + D_{yy} - k_z^2)\right)$$

B. Quadratic+ formulation

$$\hat{L}_{q_{\xi\xi}} = -\mathbf{i}k_x U_0$$
$$\hat{L}_{q_{\xi u}} = \mathbf{i}k_x \xi_0$$
$$\hat{L}_{q_{\xi v}} = -\xi_0' + \xi_0 D_y$$
$$\hat{L}_{q_{\xi w}} = \mathbf{i}k_z \xi_0$$
$$\hat{L}_{q_{\xi p}} = 0$$
$$\hat{L}_{q_{u\xi}} = \frac{\xi_0}{Re}\left(\eta_1 + \eta_2 D_y\right)$$
$$\hat{L}_{q_{uu}} = -\mathbf{i}k_x U_0 - \frac{\xi_0}{Re}\left[\eta_0\left(\frac{4}{3}k_x^2 - D_{yy} + k_z^2\right) - \eta_0' D_y\right]$$
$$\hat{L}_{q_{uv}} = -U_0' + \mathbf{i}k_x \frac{\xi_0}{3Re}\left[\eta_0 D_y + 3\eta_0'\right]$$
$$\hat{L}_{q_{uw}} = -k_x k_z \frac{\xi_0\eta_0}{3Re}$$
$$\hat{L}_{q_{up}} = -\mathbf{i}k_x \frac{\xi_0}{\gamma M_r^2} + \frac{\xi_0}{Re}\left(\eta_1\xi_0 + \eta_2\xi_0' + \eta_2\xi_0 D_y\right)$$
$$\hat{L}_{q_{v\xi}} = \mathbf{i}k_x \frac{\xi_0}{Re}\eta_{T_0}U_0'$$
$$\hat{L}_{q_{vu}} = \mathbf{i}k_x \frac{\xi_0}{3Re}\left[\eta_0 D_y - 2\eta_0'\right]$$
$$\hat{L}_{q_{vv}} = -\mathbf{i}k_x U_0 - \frac{\xi_0}{Re}\left[\eta_0\left(k_x^2 - \frac{4}{3}D_{yy} + k_z^2\right) - \frac{4}{3}\eta_0' D_y\right]$$
$$\hat{L}_{q_{vw}} = \mathbf{i}k_z \frac{\xi_0}{3Re}\left[\eta_0 D_y - 2\eta_0'\right]$$
$$\hat{L}_{q_{vp}} = -\frac{\xi_0}{\gamma M_r^2}D_y + \mathbf{i}k_x \frac{\xi_0}{Re}\eta_{T_0}U_0'\xi_0$$
$$\hat{L}_{q_{w\xi}} = 0$$
$$\hat{L}_{q_{wu}} = -k_x k_z \frac{\xi_0\eta_0}{3Re}$$
$$\hat{L}_{q_{wv}} = \mathbf{i}k_z \frac{\xi_0}{3Re}\left[\eta_0 D_y + 3\eta_0'\right]$$
$$\hat{L}_{q_{ww}} = -\mathbf{i}k_x U_0 - \frac{\xi_0}{Re}\left[\eta_0\left(k_x^2 - D_{yy} + \frac{4}{3}k_z^2\right) - \eta_0' D_y\right]$$

$$\hat{L}_{q_{wp}} = -\mathbf{i}k_z \frac{\xi_0}{\gamma M_r^2}$$

$$\hat{L}_{q_{p\xi}} = \frac{\gamma(\gamma-1)M_r^2}{Re}\eta_{T_0}(U_0')^2 + \left(\frac{\gamma}{RePr}\right)\left[\eta_0\left(-k_x^2 + D_{yy} - k_z^2\right) + \eta_0' D_y + \eta_3 + \eta_{T_0}\xi_0' D_y\right]$$

$$\hat{L}_{q_{pu}} = -\mathbf{i}k_x\gamma + \frac{\gamma(\gamma-1)M_r^2}{Re}\left(2U_0'\eta_0\right)D_y$$

$$\hat{L}_{q_{pv}} = -\gamma D_y + \mathbf{i}k_x\frac{\gamma(\gamma-1)M_r^2}{Re}\left(2U_0'\eta_0\right)$$

$$\hat{L}_{q_{pw}} = -\mathbf{i}k_z\gamma$$

$$\hat{L}_{q_{pp}} = -\mathbf{i}k_x U_0 + \frac{\gamma(\gamma-1)M_r^2}{Re}\eta_{T_0}(U_0')^2\xi_0 + \frac{\gamma}{RePr}\left\{\eta_0\left[\xi_0'' + 2\xi_0' D_y - \xi_0\left(k_x^2 - D_{yy} + k_z^2\right)\right] + \eta_0'(\xi_0' + \xi_0 D_y)\right\}$$
$$+ \frac{\gamma}{RePr}\left(\eta_3\xi_0 + \eta_{T_0}\xi_0\xi_0' D_y + \eta_{T_0}(\xi_0')^2\right)$$